



## An assessment of Arctic Ocean freshwater content changes from the 1990s to the 2006–2008 period

Benjamin Rabe <sup>a,\*</sup>, Michael Karcher <sup>a</sup>, Ursula Schauer <sup>a</sup>, John M. Toole <sup>b</sup>, Richard A. Krishfield <sup>b</sup>, Sergey Pisarev <sup>c</sup>, Frank Kauker <sup>a</sup>, Rüdiger Gerdes <sup>a</sup>, Takashi Kikuchi <sup>d</sup>

<sup>a</sup> Alfred Wegener Institute for Polar and Marine Research, Bussestr. 24, Postfach 120161, 27515 Bremerhaven, Germany

<sup>b</sup> Woods Hole Oceanographic Institution, USA

<sup>c</sup> Shirshov Institute of Oceanology, Russia

<sup>d</sup> Japan Agency for Marine-Earth Science and Technology, Japan

### ARTICLE INFO

#### Article history:

Received 21 December 2009

Received in revised form

7 November 2010

Accepted 2 December 2010

Available online 15 December 2010

#### Keywords:

Arctic

Freshwater

Observation

Model

IPY

Upper ocean

### ABSTRACT

Unprecedented summer-season sampling of the Arctic Ocean during the period 2006–2008 makes possible a quasi-synoptic estimate of liquid freshwater (LFW) inventories in the Arctic Ocean basins. In comparison to observations from 1992 to 1999, LFW content relative to a salinity of 35 in the layer from the surface to the 34 isohaline increased by  $8400 \pm 2000 \text{ km}^3$  in the Arctic Ocean (water depth greater than 500 m). This is close to the annual export of freshwater (liquid and solid) from the Arctic Ocean reported in the literature.

Observations and a model simulation show regional variations in LFW were both due to changes in the depth of the lower halocline, often forced by regional wind-induced Ekman pumping, and a mean freshening of the water column above this depth, associated with an increased net sea ice melt and advection of increased amounts of river water from the Siberian shelves. Over the whole Arctic Ocean, changes in the observed mean salinity above the 34 isohaline dominated estimated changes in LFW content; the contribution to LFW change by bounding isohaline depth changes was less than a quarter of the salinity contribution, and non-linear effects due to both factors were negligible.

© 2010 Elsevier Ltd. All rights reserved.

### 1. Introduction

Liquid freshwater (LFW) plays a major role in the Arctic Ocean: the vertical stratification in the halocline between the fresh surface layer and the salty, warm Atlantic Water (e.g. Rudels et al., 2004) limits the upward transfer of heat and thus influences the formation and melting of sea ice (e.g. MacDonald, 2000). LFW affects not only the Arctic Ocean circulation but also influences the circulation in the Atlantic, as it is exported via the Fram Strait and the passages of the Canadian Arctic Archipelago into regions of deep water formation in the Nordic Seas and the North Atlantic (Gerdes et al., 2008). Model studies have shown that this LFW export influences the large scale ocean circulation, such as the Meridional Overturning Circulation (MOC; e.g. Koenigk et al., 2007; Rennermalm et al., 2007) and the horizontal gyres (Brauch and Gerdes, 2005). LFW from the Arctic thus has a direct impact on climate (Häkkinen, 1999; Haak et al., 2003).

The LFW budget of the Arctic Ocean (Serreze et al., 2006; Dickson et al., 2007) consists of inputs from Eurasian and North American river runoff, the Norwegian coastal current via the Eurasian shelves,

precipitation, ice melt and the inflow from the Pacific through the Bering Strait; sinks of LFW are the export through the Canadian Arctic Archipelago and the western Fram Strait, and the formation and export of sea ice. Inflow of saline Atlantic Water (AW) occurs through the eastern Fram Strait and, in modified form, via the Barents Sea. The variability of this LFW budget, for instance the storage and export of LFW in the Arctic Ocean and the Nordic Seas (e.g. Häkkinen and Proshutinsky, 2004), is still not fully understood. From observations, (Curry and Mauritzen, 2005) found that  $19\,000 \pm 5\,000 \text{ km}^3$  of freshwater<sup>1</sup> were added to the Nordic Seas and the Subpolar North Atlantic basins between the early 1960s and the 1990s. Model studies have shown two strong negative anomalies in LFW export from the Arctic between 1970 and the mid 1990s. On average, the annual LFW export, referenced to a salinity of 35, was  $500 \text{ km}^3$  higher between 1970 and 1995 than during the second half of the 20th century, when the time-mean export was  $3050 \text{ km}^3/\text{y}$  (Köberle and Gerdes, 2007; Gerdes et al., 2008). The increased export represents a potential loss of LFW for the Arctic Ocean of  $12\,500 \text{ km}^3$  between 1970 and 1995, close to the decline in the

\* Corresponding author. Tel.: +49 471 4831 2403; fax: +49 471 4831 1797.  
E-mail addresses: benrabe@benrabe.de, Benjamin.Rabe@awi.de (B. Rabe).

<sup>1</sup> They used the time average salinities from the 1950s in discrete layers as reference salinities to calculate the freshwater anomaly relative to that time period.

Arctic Ocean LFW reservoir in the model experiments during this time period and comparable to the LFW gain for the Nordic Seas and the Subpolar Basins described by Curry and Mauritzen (2005). Subsequent to 1995, the model studies show an accumulation of LFW in the Arctic Ocean and a decrease in LFW export up to 2001. On the other hand, an analysis of mooring-based and ship-based observations estimates the export of LFW from the Arctic Ocean through the western Fram Strait to be approximately constant between 1998 and 2008 (de Steur et al., 2009).

During the 1990s the pathways of Pacific Water (PW) and Eurasian river water through the central Arctic changed relative to the prevailing conditions during the previous 40 years (Steele et al., 2004; Karcher et al., 2006; Newton et al., 2008). Model studies indicate that the changes in the hydrography and circulation in the Arctic Ocean covary with large scale sea surface pressure and wind stress patterns (e.g. Proshutinsky and Johnson, 1997; Dukhovskoy et al., 2004). Proshutinsky et al. (2009) analyzed observations in the Beaufort Gyre, which extends over the Beaufort Sea, the southern Canada Basin and often over parts of the Chukchi Plateau (CP; Fig. 1). Their observations during July/August/September (JAS)

from 1950 to 2007 show pronounced decadal variability and indicate a shift of the center of the gyre related to the large scale wind field. In an analysis based on the sparse observational data available over the past 100 years, Polyakov et al. (2008) infer a decrease in LFW in the Arctic Ocean from the mid-1960s to the mid-1990s. They attribute this to enhanced ice production and increased export of LFW driven by atmospheric circulation.

In this study, we analyze changes between two recent decades, making use of the unprecedented observational coverage during the International Polar Year (2006–2008) and observations over a longer time period during the 1990s. The data coverage allows us, for the first time, to use objective analysis to estimate not only the large scale spatial distribution of LFW and the LFW content but also quantify the error associated with these estimates. We focus on LFW calculated from salinity observations in the upper 500 m of the whole deep Arctic Ocean bounded by the 500 m isobath (Fig. 1). Only observations during JAS are considered, as the year-round data coverage is strongly biased toward these months. The results will be put in context with other observations, underlying physical processes and output from a simulation with a coupled ice-ocean

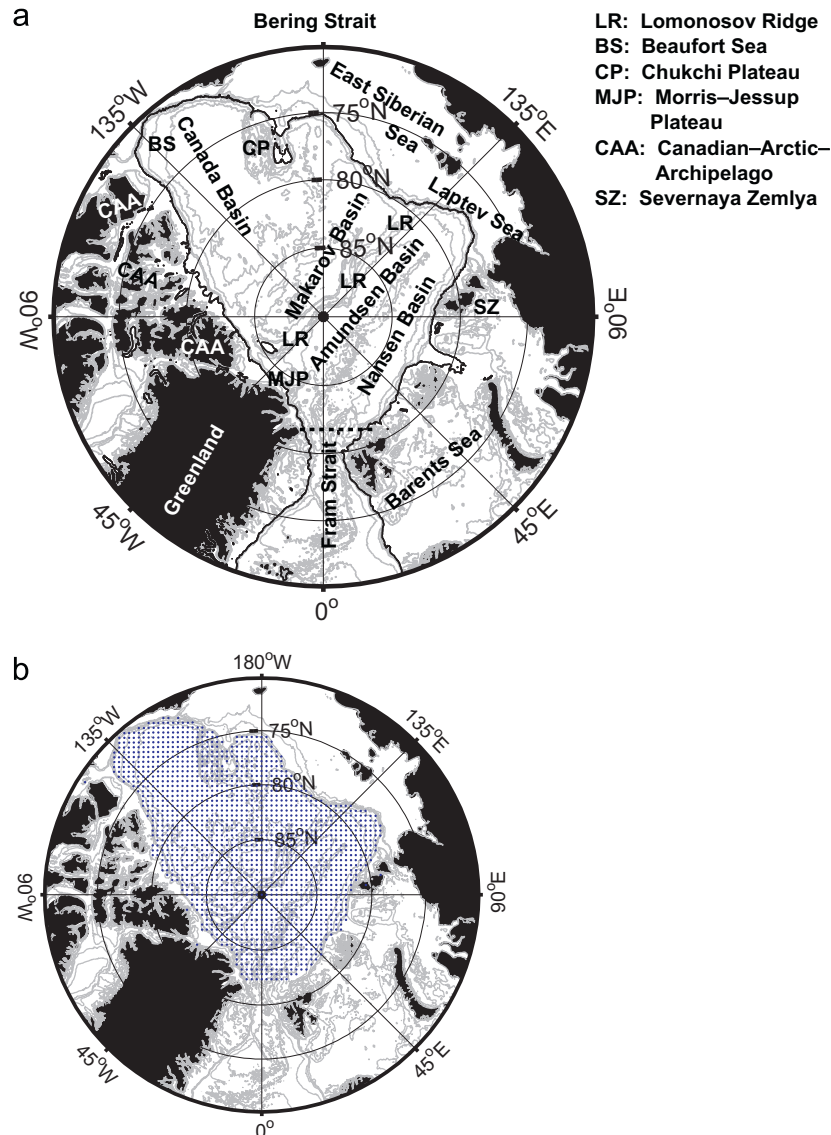


**Fig. 1.** Bathymetry of the Arctic Ocean from the IBCAO database (IBCAO Jakobsson et al., 2008): (a) geographic names; gray contour lines represent the bathymetric depths 100, 200, 500, 750, 1000, 2000, 3000 and 4000 m. The 500 m isobath represents the boundary of our “deep Arctic Ocean” domain and is shown as a thick black line; additionally, the domain was restricted to north of 82°N north of the Fram Strait (dashed line). Whenever we refer to the “North American Basin” and the “Eurasian Basin” it incorporates the Makarov and Canada basins and the Amundsen and Nansen basins, respectively. (b) Grid used for objective mapping.

general circulation model, the North Atlantic/Arctic Ocean Sea Ice model (NAOSIM; Karcher et al., 2003).

## 2. Methods

### 2.1. Observations

Salinity ( $S$ ) profile data are taken from Conductivity Temperature Depth (CTD) and Expendable CTD (XCTD) observations from ships, submarines and ice drifting stations. Since 2004, these data have been augmented by autonomous measurements (Kikuchi et al., 2007; Krishfield et al., 2008), which, around the time of the International Polar Year (IPY; 2007–2009), lead to an Arctic-wide coverage of measurements. The list of sources is given in Table 1. Despite the increasing number of observations from autonomous platforms there is a strong bias of data coverage toward Arctic summer. In order to avoid obscuring interannual variability with an unresolved seasonal cycle we use only data from JAS. Data used from the World Ocean Dataset 2009 (WOD09; Boyer et al., 2009) are taken from the “CTD” part of the database (“High-resolution Conductivity-Temperature-Depth/XCTD data”, as listed in the WOD09 documentation enclosed in the dataset). The accuracy of salinity observations is around 0.01 for XCTD after calibration with ship CTD profiles (Itoh and Shimada, 2003; Kikuchi, 2008) and the same for calibrated autonomous measurements. The manufacturer's stated accuracies for XCTD and Submerged Ship XCTD (SSXCTD) are 0.04 and 0.05, respectively. Where available, XCTD profiles that had been calibrated against conventional CTD profiles, reducing the error by a factor of two or more, were used. The accuracy of CTD casts from ships, calibrated against simultaneous water bottle samples, is generally an order of magnitude better than those of autonomous or expendable systems.

All observational data, also those taken from publicly accessible databases, were scrutinized to eliminate errors. Processing and quality control of the dataset are described in Appendix A and errors are discussed in Appendix B.

### 2.2. LFW calculations

To obtain a measure of LFW in the upper Arctic Ocean, the fraction of LFW content,  $f$ , relative to a reference salinity,  $S_{ref}$  (see also Aagaard and Carmack, 1989), was calculated between the surface

and the depth of the 34 isohaline,  $h=z(S=34)$ . This isohaline lies within the lower halocline, which has been shown to be largely unaltered by surface salinity throughout most of the Arctic Ocean (Rudels et al., 2004). The inventory of LFW in the layer above this isohaline is given by

$$h_{fw} = \int_{z=0 \text{ m}}^h f dz = \int_{z=0 \text{ m}}^h \frac{S_{ref}-S}{S_{ref}} dz, \quad (1)$$

where  $f$  is the fraction of LFW,  $S$  is the observed salinity and  $S_{ref}=35$ , approximately the salinity of the AW inflow into the Arctic Ocean via the Fram Strait and the Barents Sea; using a reference salinity of 34.8 does not significantly change  $h_{fw}$  (see also Appendix B). River water, PW, net precipitation and ice melt are additions of LFW to the AW reference, whereas ice formation is a LFW sink. The maximum error in  $f$  due to accuracy of the salinity observations is about  $2.5 \times 10^{-3}$ . In cases where parts of the profile near the surface were not measured, the shallowest data point was used for constant extrapolation to the surface, making a mixed layer assumption. The maximum pressure of this data gap was set to 20 dbar, although most profiles have data from at least 8 dbar (the potential error of this assumption is discussed in Appendix B).

Different subsets of the observations were objectively mapped to obtain the horizontal distribution of  $h_{fw}$  on a regular grid. The procedure is outlined in the following section. The mapped fields of  $h_{fw}$  for the whole deep Arctic Ocean bounded by the 500 m isobath (Fig. 1) were spatially integrated to obtain the LFW content between the ocean surface and  $h$ :

$$LFWC = \oint h_{fw} dA, \quad (2)$$

where  $dA$  is the area associated with each grid point.  $h_{fw}$  and LFWC were calculated both from the observations and from output of the NAOSIM simulation.

### 2.3. Objective mapping

To obtain horizontal maps of  $h_{fw}$  for selected time periods, subsets of the observations were objectively mapped (e.g. Bretherton et al., 1976) onto a uniform grid with 50 km distance between grid points. Our procedure is similar to that used by Böhme and Send (2005) and Böhme et al. (2008). Following McIntosh (1990), the objective estimate of a parameter  $O$  at a grid

**Table 1**

Data sources for salinity observations during JAS. The autonomous measurements were undertaken using the Ice-Tethered Profiler (ITP) and the Polar Ocean Profiling System (POPS). Data taken from the online World Ocean Database 2009 (WOD09; Boyer et al., 2009) were used to augment but not replace profiles from the other datasets listed in the table. SCICEX data from the SAIC project were used, where available, to replace profiles from the 1997 and 1998 SCICEX expeditions downloadable from EOL. The SCICEX 1993 data from EOL were preferred over those from SAIC due to more advanced processing.

Expedition, project or institute	Year(s)	Platform	Source URL or contact
World Ocean Database 2009	1992–1999	Various	<a href="http://www.nodc.noaa.gov/OC5/WOD09">http://www.nodc.noaa.gov/OC5/WOD09</a>
Scientific Ice Exercises (SCICEX)	1993	US submarines	<a href="http://data.eol.ucar.edu/codiac/dss/id=106.arcss072/">http://data.eol.ucar.edu/codiac/dss/id=106.arcss072/</a>
ARK IX/4	1993	RV Polarstern	<a href="http://www.pangaea.de/">http://www.pangaea.de/</a>
ARK XI	1995	RV Polarstern	<a href="http://www.pangaea.de/">http://www.pangaea.de/</a>
ARK XII	1996	RV Polarstern	<a href="http://www.pangaea.de/">http://www.pangaea.de/</a>
Scientific Ice Exercises (SCICEX)	1996, 1997 and 1998	US submarines	SAIC project, Sergey Pisarev ( <a href="mailto:pisarev@ocean.ru">pisarev@ocean.ru</a> )
ARK XIII	1997	RV Polarstern	<a href="http://www.pangaea.de/">http://www.pangaea.de/</a>
Scientific Ice Exercises (SCICEX)	1997 and 1998	US submarines	<a href="http://data.eol.ucar.edu/codiac/dss/id=106.arcss064/">http://data.eol.ucar.edu/codiac/dss/id=106.arcss064/</a>
ARK XV	1999	RV Polarstern	<a href="http://www.pangaea.de/">http://www.pangaea.de/</a>
Beaufort Gyre Project	2006–2008	Various ships	<a href="http://www.whoi.edu/beaufortgyre/">http://www.whoi.edu/beaufortgyre/</a>
European Union project DAMOCLES	2006–2008	POPS	<a href="http://www.ipav.fr/damocles/">http://www.ipav.fr/damocles/</a>
ARGO	2006–2008	POPS	<a href="http://www.coriolis.eu.org/cdc/argo.htm">http://www.coriolis.eu.org/cdc/argo.htm</a>
Woods Hole Oceanographic Institution (WHOI)	2006–2008	ITP	<a href="http://www.whoi.edu/itp">http://www.whoi.edu/itp</a>
ARK XXII/2 (SPACE)	2007	RV Polarstern	<a href="http://www.pangaea.de/">http://www.pangaea.de/</a>
LOMROG 2007	2007	RV Oden	Göran Björk ( <a href="mailto:gobj@gvc.gu.se">gobj@gvc.gu.se</a> )
Nansen/Amundsen Basins Observ. System (NABOS)	2007, 2008	Various ships	<a href="http://nabos.iarc.uit.edu/">http://nabos.iarc.uit.edu/</a>
ARK XXIII/3 (AMEX I)	2008	RV Polarstern	<a href="http://www.pangaea.de/">http://www.pangaea.de/</a>
Arctic Summer Cloud Ocean Study (ASCOS)	2008	RV Oden	<a href="http://www.ascos.se">http://www.ascos.se</a> (Anders Sirevaag)

point  $g$  can be obtained from a set of observations,  $O_d$ :

$$O_g = \langle O_d \rangle + \omega \cdot (O_d - \langle O_d \rangle); \quad \omega = C_{dg} \cdot (C_{dd} + I \cdot \langle \eta^2 \rangle)^{-1}, \quad (3)$$

where subscripts  $d$  and  $g$  refer to the observational (data) points and the grid points, respectively,  $\langle O_d \rangle$  is the mean of  $O_d$ , calculated as in Owens and Wong (2009) and Bretherton et al. (1976),  $\omega$  is the weighting function and  $I$  is the identity matrix. The last term is the noise variance,

$$\langle \eta^2 \rangle = \frac{\sum [n][i=1](x_i - x_{ic})^2}{2n}, \quad (4)$$

which is the mean of the squared deviation of each individual point in  $O_d(i)$  from its nearest neighbor in  $O_d(ic)$ , in terms of the mapping scales (e.g. Holbrook and Bindoff, 2000). This term measures the variations between close-by data, which is different to the signal variance that measures the squared deviation of the data from the mean.  $C_{dg}$  is the data-grid covariance and  $C_{dd}$  the data-data covariance. The interpolation (mapping) uses a Gaussian covariance function containing isotropic horizontal distance,  $D$ , and barotropic potential vorticity,  $PV$  (Davis, 1998):

$$PV = \frac{\left| \frac{f_d}{Z_d} - \frac{f_g}{Z_g} \right|}{\sqrt{\frac{f_d^2}{Z_d} + \frac{f_g^2}{Z_g}}}; \quad D = |xy_d - xy_g|, \quad (5)$$

where  $xy$  is the geographic location,  $f$  the Coriolis parameter and  $Z$  the bathymetric depth, based on the International Bathymetric Chart of the Arctic Ocean (IBCAO, Jakobsson et al., 2008). The covariance is given by

$$C = \langle s^2 \rangle \exp^{-(D^2/L^2 + PV^2/\Phi^2)}, \quad (6)$$

where the signal variance  $\langle s^2 \rangle = \sum_{n=1}^{i=1} (O_d - \langle O_d \rangle)^2/n$ ,  $L$  represents the Gaussian decorrelation scale (e-folding scale) for  $D$  and  $\Phi$  the scale for  $PV$ .

To avoid bias in the objective estimate, a reference field is often subtracted from the data before mapping. Therefore, we used Eq. (4) in a two-stage procedure: First, a very smooth map of  $O_g$  was produced. Second, the residuals between each observed value and the mapped field were mapped using smaller spatial scales to give weight to the observations closest to each grid point. Finally, the mapped residuals were added to the mapped values from the first stage to obtain the horizontal map of  $O_g$ . We separately mapped the observed  $h_{fw}$  and  $h$ . For the first stage mapping we used decorrelation scales of  $L=600$  km for horizontal distance and  $\Phi=1$  to adjust the isotropic distance scale to account for changes in barotropic potential vorticity, whereas the second stage used  $L=300$  km,  $\Phi=0.4$ . A distance of 300 km has been shown to be the appropriate decorrelation scale for LFW observations in the Canada Basin (Proshutinsky et al., 2009). Using  $\Phi=0.4$  for the non-isotropic potential vorticity scaling means that a depth change from around 3000 to 1500 m at 85° latitude sets the decay scale of the Gaussian covariance, i.e. typical bathymetric changes between deep Arctic basins and continental slopes or ridges. The combination of both the distance and potential vorticity scales leads to non-isotropic weighting contours around each grid point. For both mapping stages, only data within the large decorrelation scales from the grid point were used. If more than 60 data points were available, the data were subselected: 1/3 were randomly chosen to avoid bias toward closely spaced profiles, such as from the Ice-Tethered Profilers (ITPs). The remaining 2/3 were chosen by the highest weights ( $\omega$ , Eq. (4)), where 1/3 lied within the small decorrelation scale and 1/3 within the large scale; note that at each grid point the covariance (and weighting) functions based on the large and the small scales do not necessarily have the same shape. Observations from JAS were mapped separately for the time periods 1992–1999 and 2006–2008.

To reduce errors in the maps of the LFW inventories, a gross range limit was used for all observed LFW inventories. Furthermore, regional outliers in the observed LFW inventories, as could be caused by eddies, were eliminated. For this purpose, each observed LFW inventory was compared to the mean of the inventories within a 600 km radius. This mean and the standard deviation was calculated from all data or, if there were more than 60 data points, from a subset selected from within the 600 km and a 100 km radius in a similar way as during the mapping procedure. Each individual inventory was discarded if it was more than two standard deviations away from the mean or if the difference between the inventory and the mean was more than 7 m. A similar outlier elimination was applied to the depth of the 34 isohaline,  $h$ , prior to mapping. Finally, 858 profiles were used for the objective mapping for the time period 1992–1999 and 4299 for 2006–2008, the number for the latter period being greater mainly due to the frequent sampling of the autonomous CTD systems and increased observational efforts during the IPY.

A detailed analysis of the errors is given in Appendix B.

## 2.4. Numerical simulation

The numerical simulation was performed with the coupled ice-ocean model NAOSIM, which derives from the Geophysical Fluid Dynamics Laboratory modular ocean model MOM-2 (Pacanowski, 1995). The model domain contains the Arctic Ocean, the Nordic Seas and the Atlantic north of approximately 50°N. Open boundary conditions in the Atlantic and in the Bering Strait were formulated following Stevens (1991), allowing the outflow of tracers and the radiation of waves. For the Bering Strait a net volume inflow of 0.8 Sv has been applied. The initial and open boundary hydrography in January 1948 is taken from the PHC climatology (Steele et al., 2001), which is also used as a reference for a surface salinity restoring with 180 days timescale. The model is driven with daily atmospheric forcing from 1948 to 2008 (NCEP/NCAR reanalysis, Kalnay et al., 1996). For a more detailed description of the model see Köberle and Gerdes (2003) and Kauker et al. (2003). In an earlier model version NAOSIM has also been used to study freshwater dynamics of the Arctic Ocean (Kärcher et al., 2005; Gerdes et al., 2008; Rabe et al., 2009).

## 3. LFW distribution during 1992–1999 and 2006–2008

The observational maps show the maximum in the LFW inventories during JAS for both time periods in the Beaufort Sea (Fig. 2). This maximum results from the persistent anticyclonic wind field, leading to Ekman pumping and a depression of the lower halocline in the Beaufort Gyre, and an accumulation of freshwater. There is a gradual decline in LFW from the Beaufort Sea toward the Siberian shelf seas and toward the Fram Strait and the Barents Sea, where AW enters the Arctic Ocean. Data coverage was overall good, except close to the Canadian Arctic Archipelago and in parts of the eastern Beaufort Sea during 1992–1999 (Fig. 2a). Time averages of the simulated LFW inventories show similar large scale distributions as the mapped observations for the corresponding time periods (Fig. 3). However, the extrema in the Canada and Nansen basins are weaker in the simulation, in particular during 1992–1999 (Fig. 3a). Out of all the years under study, the simulation shows highest LFW inventories during 2008 (not shown).

A comparison of  $\Delta h_{fw}$  for the two periods (Fig. 2c) exhibits an increase ranging from 1 to 8 m of LFW in most of the deep Arctic Ocean except the western Nansen Basin, the eastern Amundsen Basin and part of the region north of the Canadian Arctic Archipelago. For the Beaufort Sea the changes hint at both a shift in the center of the Beaufort Gyre and an expansion of the gyre. In the central Arctic Ocean, Steele and Boyd (1998) observed a salinification in the central Arctic Ocean during the 1990s, resulting in a

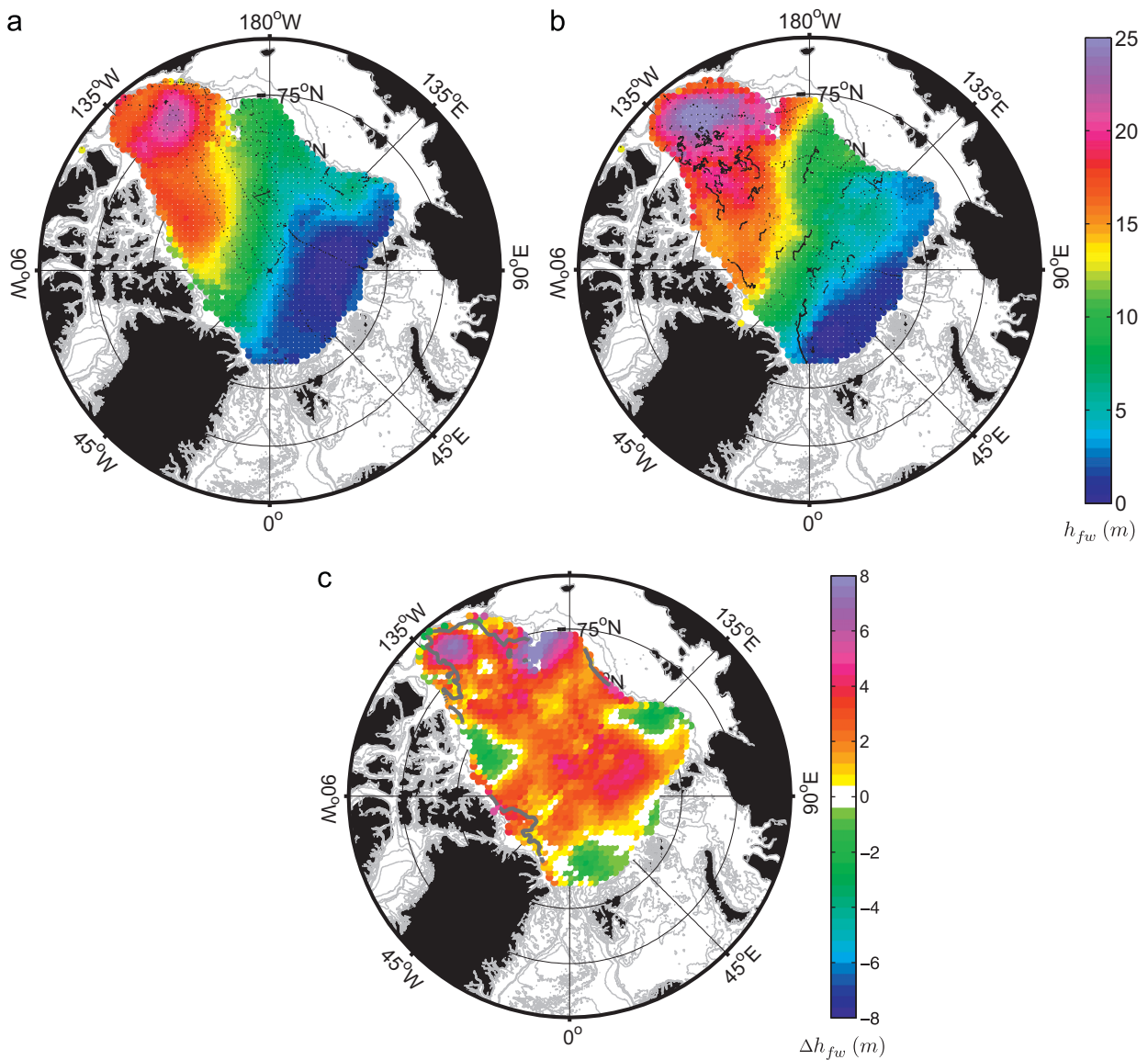


**Fig. 2.** Objectively mapped observed freshwater inventory from the surface to the depth of the 34 isohaline for the deep Arctic Ocean during JAS: (a) 1992–1999 and (b) 2006–2008. The anomaly of 2006–2008 relative to 1992–1999 is shown in (c). The locations of measured salinity profiles used for the mapping are shown as black dots in (a) and (b); larger dots are shown in Fig. 7. Only (c): values within  $\pm 0.25$  m of zero are white; the thick gray line represent the 1 m contour of the combined (maximum) statistical error estimate for both mapping time periods (see Fig. 7).

weakening of the stratification in the upper halocline. They attributed this to an eastward shift of the area influenced by fresh shelf waters. Morison et al. (2006) extended an analysis by Steele et al. (2004) up to 2005 to show that there is a 3–7 year lag in the adjustment of the upper Arctic Ocean to changes in the large scale wind field, represented by the Arctic Oscillation index. Morison et al. found that from 2000 onward, the observed hydrography of the central Arctic was again getting closer to the pre-1990s state. This was also shown by Karcher et al. (2005) in the same model simulation as used in our study. Our observations show that, regarding LFW, the trend continued up to the period 2006–2008.

A comparison of the LFW changes between the two time periods based on observations (Fig. 2c) and the simulation (Fig. 3c) shows strong similarities in the large scale pattern and amplitude. Regional differences are apparent, in particular in the Beaufort Sea and the southern Canada Basin, where the mapped observations show a shift in the LFW maximum toward the southeast; however, the lack of data north of the Canadian Arctic Archipelago during the 1990s prevents any conclusive comparison in this region. Over the whole

deep Arctic Ocean, the observed LFWC (Eq. (2)) increased by  $8400 \text{ km}^3$  between the time periods 1992–1999 and 2006–2008. This is close to the estimated total annual export of freshwater (liquid and solid) from the Arctic Ocean (Dickson et al., 2007) and almost 20% of the average of LFWC we observe for both time periods. In the simulation, LFWC changed by  $6120 \text{ km}^3$ , which is lower than the observational estimate, but of the same order of magnitude. Nevertheless, in both the observations and the simulation we see changes in the distribution of LFW summing up to an overall increase in LFWC. In the following section we investigate possible causes of these changes.

#### 4. Physical processes

##### 4.1. LFW distribution

The LFW inventories are related to two quantities: the depth of the 34 isohaline,  $h$ , and the depth averaged salinity above this

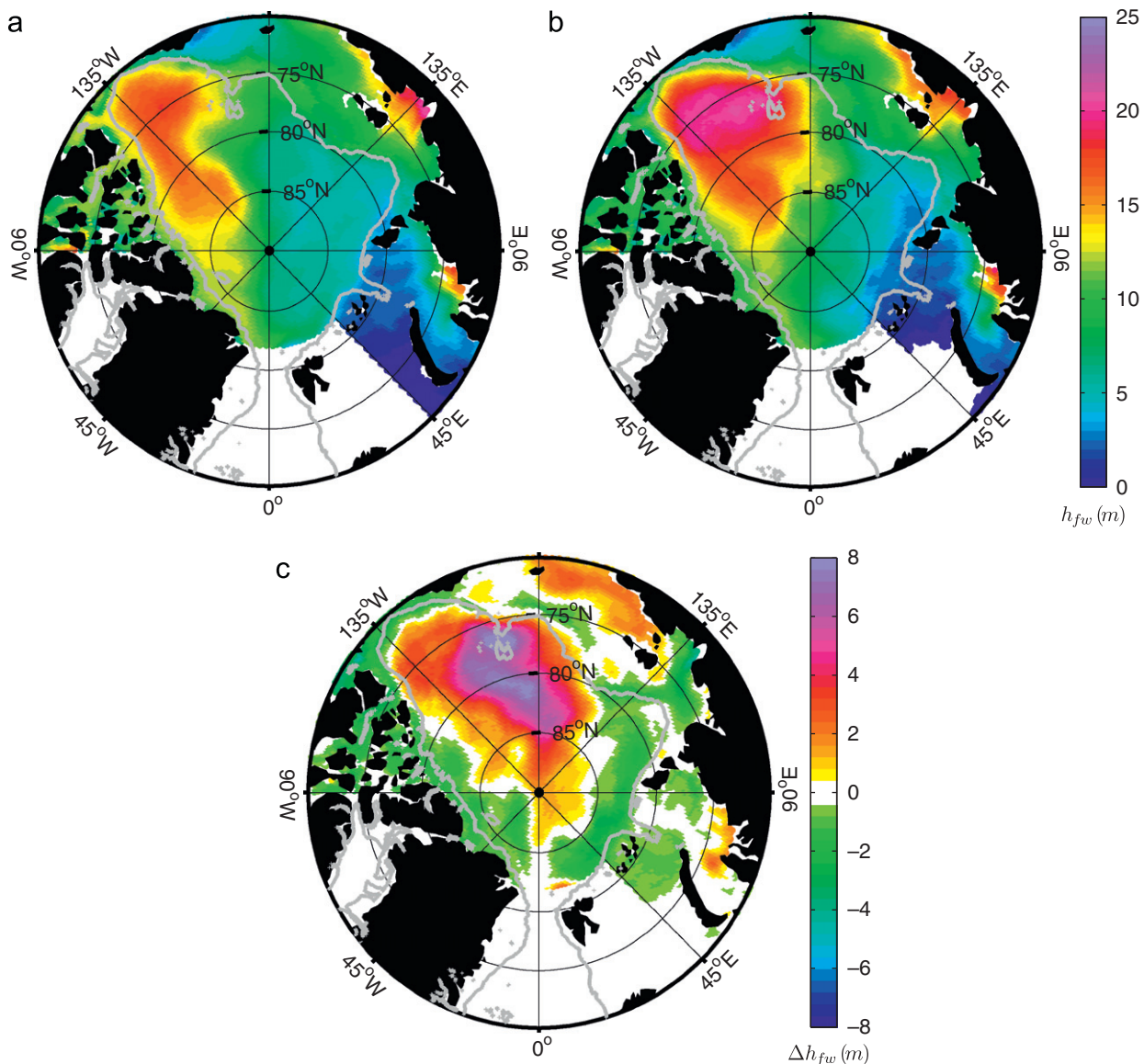


**Fig. 3.** Time averages of freshwater inventories from the surface to the depth of the 34 isohaline in the NAOSIM simulation during JAS for the time periods (a) 1992–1999 and (b) 2006–2008, and (c) the anomaly of 2006–2008 relative to 1992–1999. The thick gray line represents the 500 m isobath (IBCAO bathymetry), and the region south of 82°N in the Fram Strait is left blank, as it is not considered in the analysis.

isohaline,  $\bar{S}$ . In most parts of the deep Arctic Ocean, the 34 isohaline is sufficiently deep, so that it is unaffected by wind-induced mixing and freezing-induced convection (Rudels et al., 2004). Therefore, the differences in  $h$  between 1992–1999 and 2006–2008 ( $\Delta h$ , Fig. 4a) are likely to be the result of Ekman Pumping (EP) due to ocean surface stress induced by wind and ice motion (e.g. Yang, 2006). An exception to this is the region of the boundary current carrying AW from the Fram Strait and the Barents Sea. Here the 34 isohaline is very shallow, so that even small changes in the salinity of the AW inflow as well as changes in its temperature influencing ice formation and melt (e.g. Schauer et al., 2004) have an effect on the depth of this isohaline. Unlike EP, which is an adiabatic process, changes in  $\bar{S}$  ( $\Delta \bar{S}$ , Fig. 4b) are diabatic (non-conservative), altered by changes in the salinity of advected water or local changes in sea ice melt and formation. We split the differences in  $h_{fw}$  between the two time periods into different components:

$$\Delta h_{fw} = \overbrace{\Delta h F_1}^{\text{thickness}} + \overbrace{h_1 \Delta F}^{\text{salinity}} + \overbrace{\Delta h \Delta F}^{\text{non-linear}}, \quad (7)$$

where  $F_1 = 1 - \bar{S}_1 / S_{ref}$ ,  $\Delta F = -\Delta \bar{S} / S_{ref}$ , and the subscript 1 denotes the reference values from 199 to 1999. The three terms on the right hand side will be referred to as labeled.

The 34 isohaline shallowed slightly in the central and eastern Canada Basin, i.e. the northeastern part of the Beaufort Gyre, and parts of the central Arctic (Fig. 4a), whereas a distinct deepening can be seen around the Chukchi Plateau and in parts of the Makarov and Eurasian basins; deepening was less pronounced in the southeastern Beaufort Gyre. The effect on changes in the LFW inventories, given by the thickness term in Eq. (7) (Fig. 4c), is strongest around the Chukchi Plateau. The distribution of changes in  $h$  in the simulation (Fig. 5a) shows good agreement with the observations on the large scale; in particular, north of the Bering Strait, both the simulation and the observations show an increase in  $h$  (Figs. 5a and 4a), with a small east–west offset in the maximum. Different tendencies can be found north of Severnaya Zemlya in the Eurasian Basin and north of Greenland, where the mapped observations indicate a sinking of the halocline, while the simulation shows a rising.

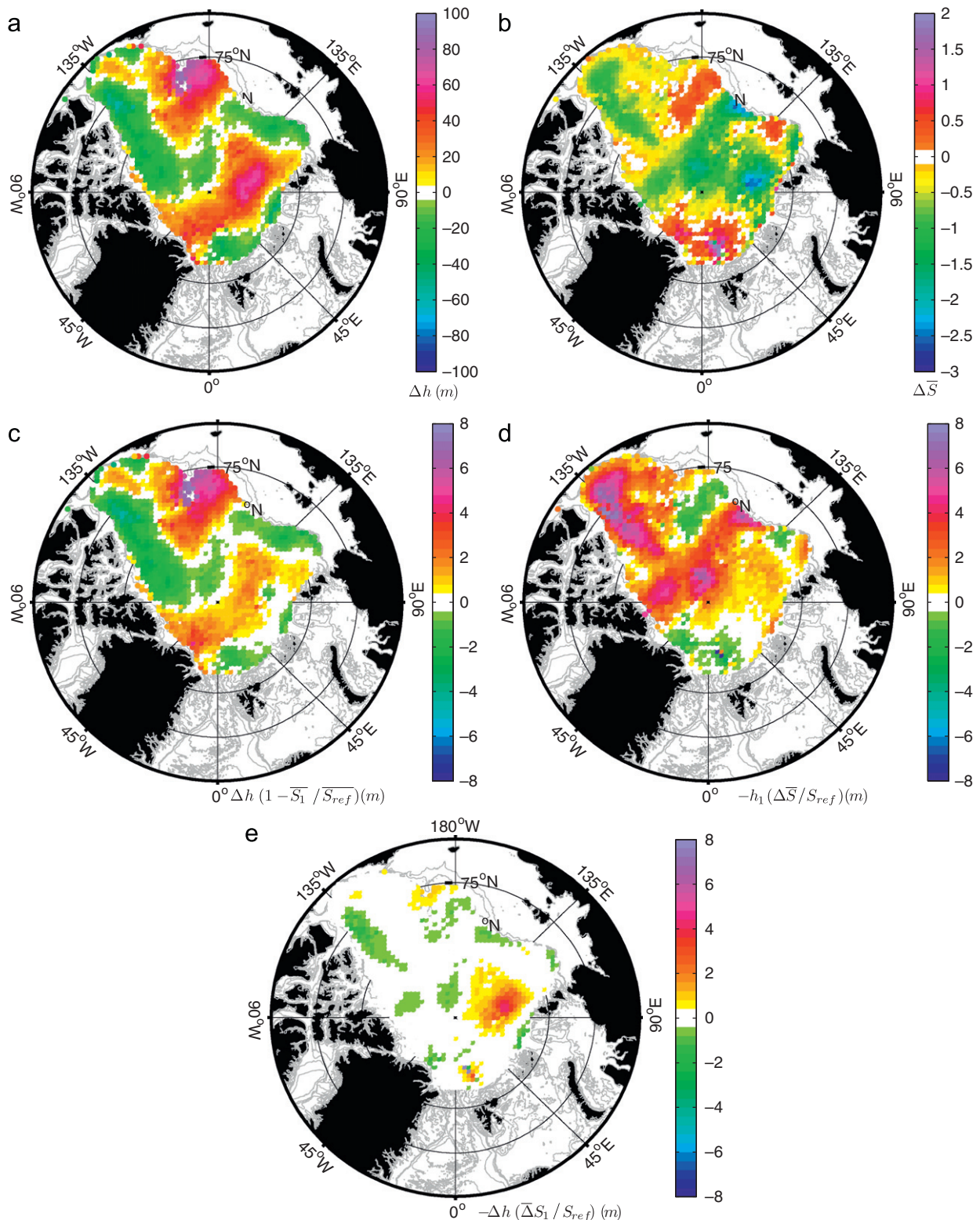


**Fig. 4.** Difference between 2006–2008 and 1992–1999 from observations in the deep Arctic Ocean during JAS of (a) the depth of the 34 isohaline,  $h=z(S=34)$ , and (b) the mean salinity above the 34 isohaline. (c), (d) and (e) show the “thickness”, “salinity” and “non-linear” terms in Eq. (7), respectively. Values within  $\pm 0.25$  m (a and c to e) or  $\pm 0.125$  (b) of zero are white.

For a calculation of surface stress induced EP, not only the wind stress but also the effect of internal ice stress has to be taken into account. Here, we make use of the ocean surface stress from the NAOSIM ice-ocean model simulation, which is forced with daily

surface winds. The ocean surface stress comprises the joint effect of wind and internal ice stresses on the oceanic motion, and the EP calculation is based on this stress. Since even in regions of predominantly downward EP, such as the Beaufort Gyre, the

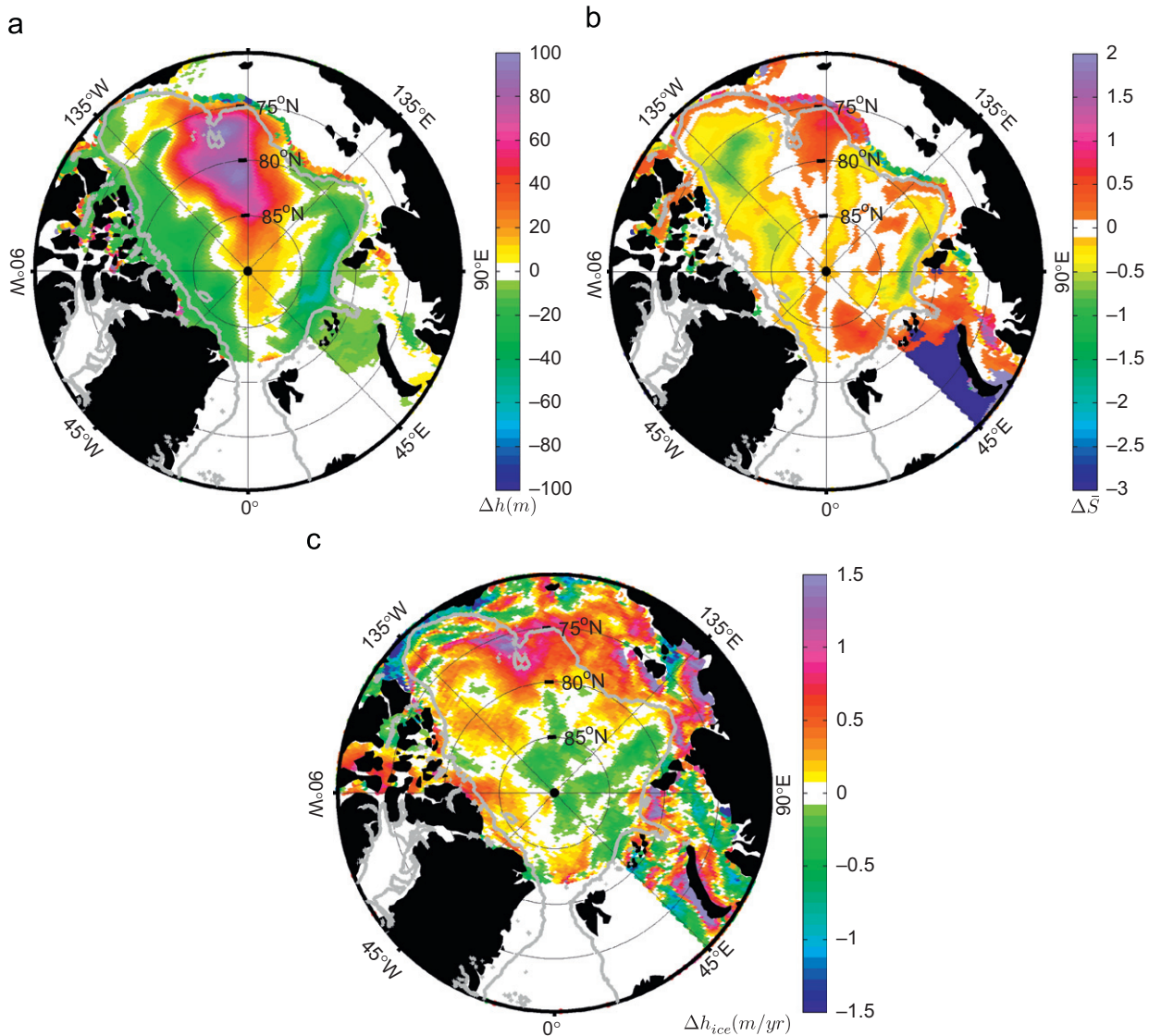


**Fig. 5.** Difference in time averages from the NAOSIM simulation between the time periods 2006–2008 and 1992–1999: (a) depth of the 34 isohaline (JAS), (b) depth-averaged salinity above this isohaline (JAS), and (c) the net sea ice melt (all year). Positive values in (d) represent a reduction in thermodynamic sea ice growth or an increase in sea ice melt. The 500 m isobath (IBCAO bathymetry) is shown as a thick gray line, and the region south of 82° N in the Fram Strait is left blank, as it is not considered in the analysis.

34 isohaline (or any other isohaline) is not displaced downward in the long term, its long-term average vertical velocity must be close to zero. The EP is counteracted by processes such as deep mixing that are not analyzed here in detail. Averaged regionally and in time over the whole 50 years of the simulation, the mean downward EP velocity is 0.5 cm/day in the North American Basin and 1.5 cm/day in the Beaufort Gyre. A comparison of the interannual variability in both regions, however, shows noticeable covariability between EP and the velocity associated with the displacement of the 34 isohaline (Fig. 6). Only for a brief period in the 1990s, local mixing and externally driven lateral advection lead, on average, to stronger discrepancies between EP and the vertical velocity of the 34 isohaline. Thus, our model simulation supports earlier studies that EP is a key process for the determination of changes in  $h$  in the Beaufort Gyre (Proshutinsky et al., 2009). In addition, our results indicate that this holds for the entire North American Basin.

In much of the deep Arctic Ocean we observe a decrease in  $\bar{S}$  (Fig. 4b) with values of  $\Delta\bar{S}$  as low as -2 in the Makarov Basin and parts of the Eurasian Basin. Around the Chukchi Plateau and near the edges of the Eurasian Basin  $\bar{S}$  increased. In the earlier period,  $h$

was lower in much of the Eurasian Basin than in the central Arctic and the Canada Basin. Therefore, the strong decreases in  $\bar{S}$  in the Eurasian Basin lead to smaller increases in the LFW inventories due to the salinity term in Eq. (7) (Fig. 4d), than elsewhere. In the simulation the increases in  $\bar{S}$  are similar to the observations north of the Bering Strait and north of the Fram Strait. The main simulated decrease is found in the Canada Basin, whereas there were weaker, localized decreases in the Eurasian Basin.

Changes in the net sea ice melt between the two time periods may have influenced  $\bar{S}$  either locally or via advection of freshwater, (salt) from ice melt (formation), for example from the shelves. From the difference in simulated net sea ice melt between 2006–2008 and 1992–1999 (Fig. 5c) we find a freshwater input from net melt around the Chukchi Plateau. This likely contributed to the decrease in salinity downstream to the east in the Beaufort Sea, evident in the maps of seen  $\bar{S}$  from the observations (Fig. 4b) and the simulation (Fig. 5b). In much of the North American Basin, on the East Siberian and Laptev sea shelves and in the basins to the north net sea ice melt increased (Fig. 5c), whereas in parts of the central Arctic and the Eurasian Basin small decreases occurred.

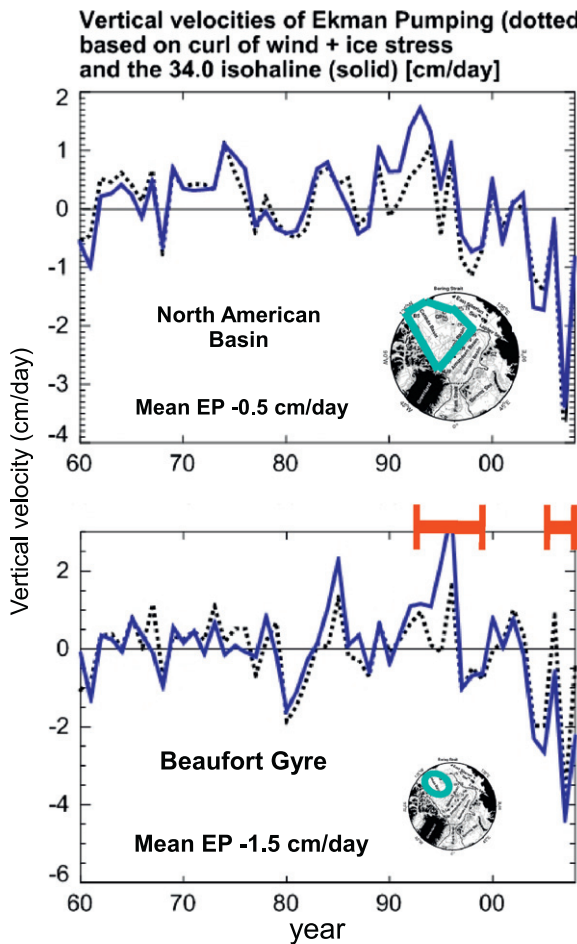


**Fig. 6.** Time series of annual mean vertical velocity (positive upward) in the NAOSIM simulation derived from Ekman Pumping (EP; dotted), based on the curl of the ocean-surface (wind and ice) stress, and from the vertical displacement of the 34.0 isohaline (solid). Shown is the spatial means for the North American Basin and the Beaufort Gyre, where the EP velocity is offset by the time mean for each region. The regions used for spatial averaging are sketched in the inlaid maps, and the x-axis shows the time from 1960 until 2008 (middle-of-year), where the two time periods under study in our FW analysis are marked as red horizontal bars.

Although we observe an overall freshening in the Canada Basin, there was a redistribution of LFW in the southern part of the Beaufort Gyre (Fig. 2c), associated with both changes in  $\Delta h$  (Fig. 4a) and in  $\bar{S}$  (Fig. 4b). Here, tracer measurements between 1987 and 2007 show less removal of LFW within the surface layer due to a reduction in winter ice formation, whereas meteoric water (river runoff and precipitation) was increasing in the center of the gyre (Yamamoto-Kawai et al., 2009); in 2006 and 2007, Yamamoto-Kawai et al. observed that also net ice melt increased in that part of the gyre. However, some of the observed increases in LFW near the surface were compensated by decreases in LFW contained in Pacific Water below (Proshutinsky et al., 2009). Thus both a changed Ekman pumping due to changing ocean surface stress and an accumulation of river water and ice melt in the North American Basin have contributed to the observed changes between the two time periods.

In large parts of the Eurasian Basin, along the Lomonosov Ridge and in the Makarov Basin, we find that the observed increase in LFW can be mostly attributed to a decrease in the observed  $\bar{S}$ . Here, the simulation indicates no significant or uniform change in net sea ice melt (Fig. 5c). Furthermore, there are indications from four years of hydrographic observations at the Lomonosov Ridge close to the

North Pole since 1990 that ice melt water was not at an extreme high in 2007 (Bert Rudels pers. comm.). Tracer measurements (Jones et al., 2008; Anderson et al., 2004) and model simulations (Karcher et al., 2006), on the other hand, suggest a change in the circulation of river water that was temporarily accumulating on the Siberian shelves and started to leave the shelves north of the East Siberian Sea around 1998; further east than previously. It subsequently replenished the 1990s LFW deficit in the central Arctic. This pulse of river water reached the Fram Strait in 2005, as observed by Rabe et al. (2009), and was also exported through the Canadian Arctic Archipelago. Observations have shown that the concentration of river water north of the Siberian Islands close to the Lomonosov Ridge was still higher in 2007 than in 1993 and 1995 (Abrahamsen et al., 2009), suggesting that also in the central Arctic the observed increases in LFW between the two time periods studied in this paper were caused by high concentrations of river water.

In summary, observations and the NAOSIM simulation indicate that the components of the changes in LFW vary by region: the shift in the LFW maximum in the Beaufort Gyre is likely a consequence of a mixture of changes in net sea ice melt, wind-ice stress induced EP and accumulation of advected river water. Around the Lomonosov Ridge, the Makarov Basin and in the Eurasian Basin the increase in river water from the Siberian shelves made the strongest contribution, whereas changes in the layer depth, although large, contributed much less. In addition, changes in layer depth in the Eurasian Basin could not be associated with EP during the 1990s in the simulation. Therefore, the freshening in the Eurasian Basin between the two time periods must have been caused by the properties and distribution of inflowing water and changes in the formation of the lower halocline. The product of changes in  $h$  and  $\bar{S}$ , represented by the last term in Eq. (7) (Fig. 4e), played a role only in small parts of the Eurasian Basin (Figs. 4c and d).

#### 4.2. LFW content

On average over the whole domain, i.e. the upper deep Arctic Ocean, the depth of the 34 isohaline increased by about 7 m effecting a volume increase of about 31 000 km<sup>3</sup>, whereas the average salinity above this isohaline decreased by about 0.5. Nevertheless, the thickness term in Eq. (7) gives an increase in LFWC by 1600 km<sup>3</sup>, whereas the salinity term results in +6500 km<sup>3</sup>. This means that changes in  $\bar{S}$  contributed much more to changes in LFWC than changes in  $h$ ; therefore, EP primarily redistributed LFW within the Arctic Ocean. The fact that the integral of the thickness-term in Eq. (7) over the whole deep Arctic Ocean is not zero may be explained by the regions where the 34 isohaline is not in the adiabatic interior or where the 34 isohaline reached onto the shelves. Furthermore, the thickness contribution is of the order of the uncertainty in the mapping process (Appendix B). On the other hand, decreases in  $\bar{S}$  originated from changes in ice formation and melt, and inflow of LFW from the shelves. The non-linear term gives an increase of less than 300 km<sup>3</sup> and is, therefore, negligible. Overall, the observed LFWC change is primarily due to changes in  $\bar{S}$ .

#### 5. Summary and conclusion

During July/August/September of 2006–2008 salinity profiles were measured across all Arctic Ocean basins within a few years. These were used to analyze the distribution of LFW above the lower halocline represented by the 34 isohaline. The measurements from 2006–2008 were compared to observations from the 1990s, where

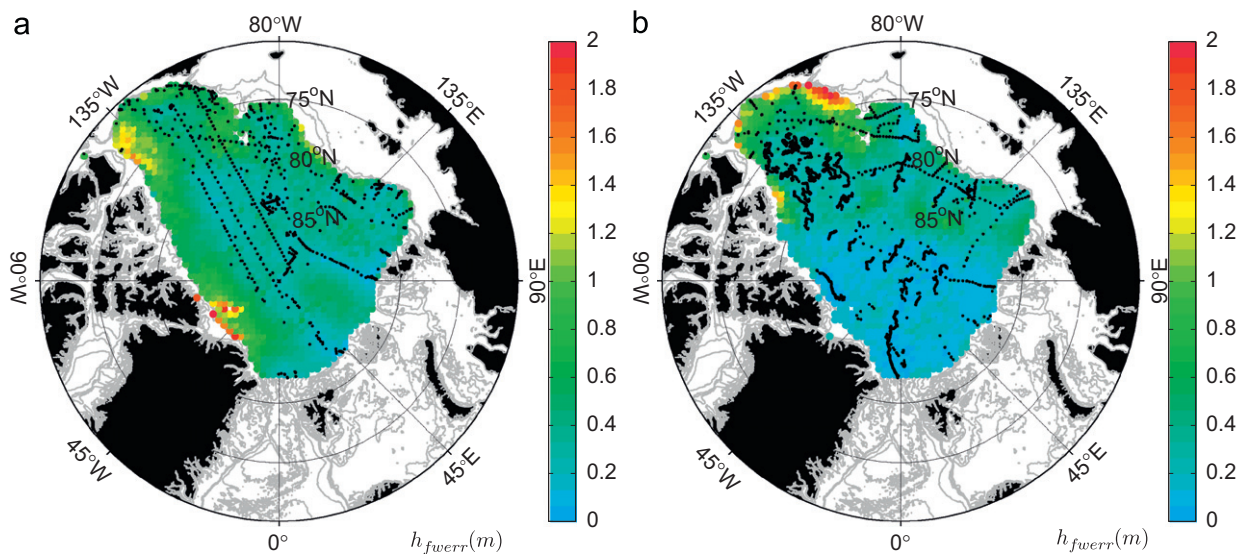


**Fig. 7.** Statistical error estimate (Eq. (8)) associated with the objective maps of freshwater inventories in Fig. 2: (a) 1992–1999 and (b) 2006–2008. The locations of measured salinity profiles used for the mapping are shown as black dots.

measurements were more sparse but still covered most of the deep Arctic Ocean.

1. The upper ocean LFW content for the deep Arctic Ocean during JAS increased by  $8400 \pm 2000 \text{ km}^3$  between 1992–1999 and 2006–2008. This is close to the annual export of freshwater (liquid and solid) to and from the Arctic Ocean and almost 20% of the average LFW content observed for both time periods.
2. The spatial pattern of LFW changes simulated by NAOSIM agrees well with the observations on large scales. The simulated LFW content change is, within the error margins, the same as what was derived from observations.
3. Over the whole domain, changes in the observed depth of the 34 isohaline lead to a redistribution of LFW and did not significantly influence the LFW content overall. In many regions, the changes in the depth of the 34 isohaline lead to changes in LFW; in particular, north of the Bering Strait, where the simulation suggests stronger anticyclonic stress during 2006–2008, leading to a downward displacement of this isohaline due to downward Ekman pumping and hence to an increase in LFW. Only in regions where the lower halocline is formed, north of the Fram Strait and the Barents Sea, and north of the Canadian Arctic Archipelago, did we observe diabatic changes in the depth of the 34 isohaline.
4. The observed LFW changes were largely due to a freshening of the layer above the 34 isohaline. In the central Arctic, this was most likely due to enhanced advection of river water advected from the shelves. In certain regions, such as north of the Bering Strait, increases in LFW can be attributed to changes in the simulated net sea ice melt. In addition, the simulation shows increases in net sea ice melt on the Siberian shelves that may have been advected into the basins.

The observed change in the LFW content is equivalent to an average annual increase of about  $750 \text{ km}^3$  between 1996 and 2007; the value in our simulation is about  $550 \text{ km}^3$ . These values are of similar magnitude as past changes seen in model studies by Köberle and Gerdes (2007) and Gerdes et al. (2008), where the LFW export from the Arctic Ocean between 1970 and 1995 was temporarily enhanced by  $500 \text{ km}^3$  annually, contributing to the LFWC decline in the Arctic over the same period. River runoff has

not changed on an Arctic-wide scale (Serreze et al., 2006). LFW transports through the Bering Strait have been shown to vary on an interannual to multi-year timescale, but no trend was observed between 1998 and 2008 (Woodgate et al., 2006, and pers. comm.). Dmitrenko et al. (2008) have argued that, on average between 1920 and 2005,  $500 \text{ km}^3/\text{yr}$  of LFW were advected from the eastern Siberian shelf to the Arctic Ocean through the northeastern Laptev Sea during times of anticyclonic atmospheric circulation. This value is again of similar order as the changes we observed. Therefore, the most likely candidates for changing the LFWC between our two time periods are the LFW exports from the Arctic to the Nordic Seas and the North Atlantic and the exchange between the upper deep Arctic Ocean and the Siberian shelves.

## Acknowledgments

We thank the participants of the various observational efforts listed in Table 1 for obtaining and processing the salinity measurements. This work was supported by the Co-Operative Project “The North Atlantic as Part of the Earth System: From System Comprehension to Analysis of Regional Impacts” funded by the German Federal Ministry for Education and Research (BMBF) and by the European Union Sixth Framework Programme project DAMOCLES (Developing Arctic Modelling and Observing Capabilities for Long-term Environment Studies), contract number 018509GOCE. This work is a contribution to the “Helmholtz Climate Initiative REKLIM” (Regional Climate Change), a joint research project by the Helmholtz Association of German research centres (HGF).

## Appendix A. Data processing procedures for salinity profiles

There are three categories of data we make use of in this study:

1. Data from ship CTDs directly obtained from the PIs only underwent a gross visual screening as these data were thoroughly processed and calibrated by the respective PIs and colleagues.
2. Data from WOD09 lying within our domain, the deep Arctic Ocean, only covers the first time period, 1992–1999. All data with a WOD flag of 1 (“outside range”) and 8 (“questionable

data") were discarded (please refer to the WOD09 manual for a description of ranges by region and depth interval; Boyer et al., 2009). Furthermore, the data were thoroughly screened for spikes, unrealistic gradients and noise in the salinity profiles as well as gross offsets in temperature-salinity space. Any erroneous data were discarded or were replaced with data of better quality, where available. For example, the SCICEX93 (Scientific Ice Expeditions, 1993) data in WOD09 is in almost raw format, but those data are also available in a more advanced stage of processing, where SSXCTD casts from the submarine under the ice were corrected using surface CTD casts from the same expedition (Morison et al., 1998).

3. Autonomous ice-based profilers, the WHOI Ice-tethered Profiler (ITP) and the MetOcean Polar Ocean Profiling System (POPS) provided a large number of profiles for 2006–2008. ITPs (Krishfield et al., 2008) obtain profile data at about 0.25 m vertical resolution (1 Hz CTD sampling rate). These data were corrected for CTD sensor lags (Johnson et al., 2007) and screened for erroneous data. Subsequently, a conductivity correction was performed by comparing the lower part of the profile with objectively mapped independently measured salinity on selected isotherms (potential temperatures {0.3, 0.4, 0.5} °C). After correction, the accuracy of the salinity data is 0.01. A detailed description of ITP processing procedures can be found in "ITP Data Processing Procedures" available at "<http://www.whoi.edu/itp/data/>". POPS (Kikuchi et al., 2007) provide data only at discrete pressure intervals, ranging from 2 dbar near the surface to 10 dbar in the lower part of the profile. Hence, sensor correction could not be applied to the POPS data, but data were thoroughly screened for errors. Subsequently, a conductivity correction was performed, using historical data as a reference in a similar way as for the ITPs. The POPS vertical resolution is still above that of ARGO profilers, which claim an accuracy of 0.01 in salinity, after conductivity correction against historical data (Owens and Wong, 2009, and references therein). Therefore, we assume this accuracy also holds for data from POPS.

Any profiles that did not meet the following criteria were discarded: data gaps ranging over more than 20 dbar for either pressures lower than 150 dbar or salinities less than 34.5; more than 30% of the data missing in the layer above the 34 isohaline. The remaining profiles were interpolated onto 2 dbar pressure levels, where interpolated values that were more than 3 dbar away from any original data point were eliminated. This avoids implausible interpolation across strongly stratified parts of the water column. Some duplicate profiles were manually identified and removed from the combined dataset. Further duplicates were eliminated in cases where more than one profile was found with the same latitude, longitude, time stamp and maximum profile pressure, within the following margins: two decimal places for latitude/longitude, six hours for time and 50 dbar for maximum profile pressure. Preference was given to profiles contained in datasets other than WOD09, if possible those obtained directly from the PIs responsible for their processing, as these data were of equal or better quality.

## Appendix B. Uncertainty in FWC estimates

The sources of error within our LFWC estimate consist of the statistical error associated with the mapping procedure, errors due to sampling gaps in regions of potentially high vertical gradients in salinity and errors due to the accuracy of the measurement devices.

The statistical mapping error is given at each grid point  $g$  by

$$\eta_g^2 = \langle s^2 \rangle - \omega \cdot C_{dg}^T + \frac{(1-\omega)^2}{\sum(C_{dd} + I \cdot \langle \eta^2 \rangle)^{-1}}, \quad (8)$$

where the symbols are defined in Section 2.3.

We found  $\eta_g$  from mapping LFW to be highest ( $> 1.5$  m) in regions without data, such as north of the Canadian Arctic Archipelago, but significant errors ( $\sim 1$  m) were also found in regions of higher data coverage in the North American Basin due to uneven spatial distribution of the profiles and variability in the data (Fig. 7). We tested the reliability of the LFWC estimate from the mapped LFW inventories by considering only grid points below an error threshold: the difference in LFWC between 2006–2008 and 1992–1999 considering only grid points with  $\eta_g < 1.5$  m is 8200 km<sup>3</sup>, and using  $\eta_g < 1$  m it is 7600 km<sup>3</sup>; here, we use the field of combined error from both time periods, considering the higher error of the two at each grid point. Considering only 1992–1999, the time period with the higher mapping error, the estimate of the error is 2000 km<sup>3</sup> using a threshold of  $< 1.5$  m, the same as that without a threshold, and 1800 km<sup>3</sup> using a threshold of  $< 1$  m. Hence, our estimate of the difference in LFWC based on mapped LFW inventories appears to be robust with respect to spatial coverage of the data. Furthermore, we performed the mapping with smaller distance scales,  $L$ , (potential vorticity scales,  $\Phi$ , were unchanged) and compared the resulting map to the one in Fig. 2c. Considering only grid points covered by both maps, we obtain a different LFWC for each comparison: First, using 100 and 50 km as the large and small distance scales, respectively, lead to a difference in LFWC between both time periods of 5000 km<sup>3</sup>. This compares to 5100 km<sup>3</sup> in the mapping with scales of 600 and 300 km. Second, mapping with 200/100 km leads to 7700 km<sup>3</sup>, which is the same as the value from the 600/300 km map. The sensitivity of the LFWC difference between the two time periods due to the fraction of randomly chosen data points in the mapping process is around 100 km<sup>3</sup>, using five independent mappings of the same data in each time period. Likewise, changing the reference salinity,  $S_{ref}$ , in Eq. (1) to 34.8 only decreases the LFWC difference by 200 km<sup>3</sup>. The sensitivity studies suggest that the difference in LFWC between both time periods is between 6000 and 10 000 km<sup>3</sup>.

Data gaps in parts of the profile with strong vertical gradients of salinity near the surface may introduce additional error to the LFW inventories and thus the LFWC. For example, autonomous profilers, tethered to an ice floe, do not sample the top 7–10 m; some other salinity profiles are missing as much as the top 20 m, the maximum allowed in our selection. We tested potential errors in two ways:

1. A set of 215 CTD-based salinity profiles from two trans-Arctic Polarstern cruises, which took stations in all the four Arctic Basins, is used. The LFW inventories using the full profiles, usually starting at 2 dbar, are compared to inventories using the value from 10 dbar in each profile as a constant to the surface. In all 215 profiles, the maximum difference between the salinity at 10 dbar and the minimum salinity in the layer to the surface is 2, and only 12% of these profiles show a salinity difference that leads to a difference in the LFW inventory of more than 0.05 m. This indicates that undersampling the upper 10 dbar leads to an error smaller than that given by the mapping procedure. One caveat of this comparison is that during CTD casts large research vessels evoke mixing of the upper 10–20 m due to the use of strong stern or bow thrusters. While this does not affect vertically integrated quantities, such as our LFW inventories, it may not fully resolve shallow layers of ice melt.
2. The LFW inventories were calculated assuming that the data was missing in a pressure interval near the surface in all profiles. We did this calculation in two ways: First, we filled the artificial gap by making a mixed layer assumption, using the shallowest data point below the gap for constant extrapolation to the surface. Second, we did not fill the artificial gap, ignoring any data within the pressure interval. Assuming a mixed layer in the pressure interval 0–10 dbar or 0–20 dbar, the resulting LFWC

differences between the two time periods are 8000 or 6800 km<sup>3</sup>, respectively. Even if we completely ignore the upper 10 or 20 dbar, we still obtain significant LFWC differences, 6700 or 4900 km<sup>3</sup>, respectively. Regardless of how we treat any near-surface sampling gaps, the large scale patterns of the differences in LFW inventories between the two time periods are similar to the one in Fig. 2c, which is why the corresponding maps are not shown here. Hence, the existence of near-surface sampling gaps does not alter our conclusion that a significant increase in LFWC occurred between 1992–1999 and 2006–2008.

## References

- Aagaard, K., Carmack, E.C., 1989. The role of sea ice and other fresh water in the Arctic circulation. *J. Geophys. Res.* 94 (C10), 14,485–14,498.
- Abrahamsen, E.P., Meredith, M.P., Falkner, K.K., Torres-Valdes, S., Leng, M.J., Alkire, M.B., Bacon, S., Laxon, S.W., Polyakov, I., Ivanov, V., 2009. Tracer-derived freshwater composition of the Siberian continental shelf and slope following the extreme Arctic summer of 2007. *Geophys. Res. Lett.* 36, L07602. doi:10.1029/2009GL037341.
- Anderson, L.G., Jutterström, S., Kaltin, S., Jones, E.P., Björk, G., 2004. Variability in river runoff distribution in the Eurasian Basin of the Arctic Ocean. *J. Geophys. Res.* 109. doi:10.1029/2003JC001773.
- Böhme, L., Send, U., 2005. Objective analyses of hydrographic data for referencing profiling float salinities in highly variable environments. *Deep-Sea Res. I* 52 (3–4), 651–664. doi:10.1016/j.dsr.2004.12.014.
- Böhme, L., Meredith, M.P., Thorpe, S.E., Biuw, M., Fedak, M., 2008. The ACC frontal system in the South Atlantic: monitoring using merged Argo and animal-borne sensor data. *J. Geophys. Res.* 113, C09012. doi:10.1029/2007JC004647.
- Boyer, T., Antonov, J.I., Baranova, O.K., Garcia, H.E., Johnson, D.R., Locarnini, R.A., Mishonov, A.V., O'Brien, T.D., Seidov, D., Smolyar, I.V., Zweng, M.M., 2009. World ocean database 2009. In: Levitus, S. (Ed.), NOAA Atlas NESDIS, vol. 66. U.S. Government Printing Office, Washington, DC, 216 pp. DVDs.
- Brauch, J.P., Gerdes, R., 2005. Reaction of the northern North Atlantic and Arctic oceans to a sudden change of the NAO. *J. Geophys. Res.* 110, C11018. doi:10.1029/2004JC002436.
- Bretherton, F.P., Davis, R.E., Fandry, C.B., 1976. A technique for objective analysis and design of oceanographic experiments applied to MODE-73. *Deep-Sea Res. I* 23, 559–582.
- Curry, R., Mauritzen, C., 2005. Dilution of the Northern North Atlantic Ocean in recent decades. *Science* 308, 1772–1774. doi:10.1126/science.1109477.
- Davis, R.E., 1998. Preliminary results from directly measuring middepth circulation in the tropical and South Pacific. *J. Geophys. Res.* 103 (C11), 24,619–24,639.
- de Steur, L., Hansen, E., Gerdes, R., Karcher, E., anFahrbach, M., Holtorf, J., 2009. Freshwater fluxes in the East Greenland Current: a decade of observations. *Geophys. Res. Lett.* 36, L23611. doi:10.1029/2009GL041278.
- Dickson, R., Rudels, B., Dye, S., Karcher, M., Meincke, J., Yashayaev, I., 2007. Current estimates of freshwater flux through Arctic and subarctic seas. *Prog. Oceanogr.* 73, 210–230. doi:10.1016/j.pocean.2006.12.003.
- Dmitrenko, I.A., Kirillov, S.A., Tremblay, L.B., 2008. The long-term and interannual variability of summer fresh water storage over the eastern Siberian shelf: implication for climatic change. *J. Geophys. Res.* 113, C03007. doi:10.1029/2007JC004304.
- Dukhovskoy, D.S., Johnson, M.A., Proshutinsky, A., 2004. Arctic decadal variability: an auto-oscillatory system of heat and fresh water exchange. *Geophys. Res. Lett.* 31, L03302. doi:10.1029/2003GL019023.
- Gerdes, R., Karcher, M., Köberle, C., Fieg, K., 2008. Simulating the long term variability of liquid freshwater export from the Arctic Ocean. In: Dickson, R.R., Meincke, J., Rhines, P. (Eds.), Arctic-Subarctic Ocean Fluxes: Defining the Role of the Northern Seas in Climate, Springer Science and Business Media, pp. 405–425 (Chapter 17).
- Haak, H., Jungclaus, U., Mikolajewicz, U., Latif, M., 2003. Formation and propagation of great salinity anomalies. *Geophys. Res. Lett.* 30, 1473. doi:10.1029/2003GL01765.
- Häkkinen, S., 1999. A simulation of the thermohaline effects of a great salinity anomaly. *J. Climate* 12, 1781–1795.
- Häkkinen, S., Proshutinsky, A., 2004. Freshwater content variability in the Arctic Ocean. *J. Geophys. Res.* 109, C03051. doi:10.1029/2003JC001940.
- Holbrook, N.J., Bindoff, N.L., 2000. A statistically efficient mapping technique for four-dimensional ocean temperature data. *J. Atmos. Ocean. Technol.* 17 (6), 831–846.
- Itoh, M., Shimada, K., 2003. XCTD salinity calibration in the Arctic Ocean, Technical Report 48, Report of Japan Marine Science and Technology Center (JAMSTEC-R), JAMSTEC, Yokosuka, Japan.
- Jacobsson, M., Macnab, R., Mayer, M., Anderson, R., Edwards, J., Hatzky, J.M., Schenke, H.-W., Johnson, P., 2008. An improved bathymetric portrayal of the Arctic Ocean: implications for ocean modeling and geological, geophysical and oceanographic analyses. *Geophys. Res. Lett.* 35. doi:10.1029/2008GL033520.
- Johnson, G.C., Toole, J.M., Lason, N.G., 2007. Sensor corrections for Sea-Bird SBE-41CP and SBE-41 CTDs. *J. Atmos. Ocean. Technol.* 24 (6), 1117–1130. doi:10.1175/JTECH2016.1.
- Jones, E.P., Anderson, L.G., Jutterström, S., Mintrop, L., Swift, J.H., 2008. Pacific fresh water, river water and sea ice meltwater across Arctic Ocean basins: results from the 2005 Beringia Expedition. *J. Geophys. Res.* 113, C08012. doi:10.1029/2007JC004124.
- Kalnay, E., et al., 1996. The NCEP/NCAR 40-Year Reanalysis Project. *Bull. Am. Meteorol. Soc.* 77 (3), 437–495.
- Kärcher, M., Gerdes, R., Kauker, F., Köberle, C., Yashayaev, I., 2005. Arctic Ocean change heralds North Atlantic freshening. *Geophys. Res. Lett.* 32. doi:10.1029/2005GL023861.
- Kärcher, M., Gerdes, R., Kauker, F., 2006. Modeling of  $\delta_{18}\text{O}$  and  $^{99}\text{Tc}$  dispersion in Arctic and subarctic seas, ASOF Newsletter, 5, available from: <<http://asof.npolar.no>>.
- Kärcher, M.J., Gerdes, R., Kauker, F., Köberle, C., 2003. Arctic warming: evolution and spreading of the 1990s warm event in the Nordic seas and the Arctic Ocean. *J. Geophys. Res.* 108 (C2). doi:10.1029/2001JC001265.
- Kauker, F., Gerdes, R., Kärcher, M., Köberle, C., Lieser, J.L., 2003. Variability of Arctic and North Atlantic sea ice: a combined analysis of model results and observations from 1978 to 2001. *J. Geophys. Res.* 108 (C6). doi:10.1029/2002JC001573.
- Kikuchi, T., 2008. XCTD observation. In: Schauer, U. (Ed.), The Expedition ARKTIS-II/2 of the Research Vessel "Polarstern" in 2007, Reports on Polar and Marine Research. Alfred-Wegener Institute for Polar and Marine Research, vol. 579, Bremerhaven, Germany, pp. 96–102.
- Kikuchi, T., Inoue, J., Langevin, D., 2007. Argo-type profiling float observations under the Arctic multiyear ice. *Deep-Sea Res. I* 54 (9), 1675–1686.
- Köberle, C., Gerdes, R., 2003. Mechanisms determining the variability of Arctic sea ice conditions and export. *J. Climate* 16, 2843–2858.
- Köberle, C., Gerdes, R., 2007. Simulated variability of the Arctic Ocean fresh water balance 1948–2001. *J. Phys. Oceanogr.* 37, 1628–1644. doi:10.1175/JPO3063.1.
- Koenigk, T., Mikolajewicz, U., Haak, H., Jungclaus, J., 2007. Arctic freshwater export in the 20th and 21st centuries. *J. Geophys. Res.* 112, G04S41. doi:10.1029/2006JC00274.
- Krishfield, R., Toole, J., Proshutinsky, A., Timmermans, M.L., 2008. Automated Ice-Tethered Profilers for seawater observations under pack ice in all seasons. *J. Atmos. Ocean. Technol.* 25, 2091–2105.
- MacDonald, R.W., 2000. Arctic estuaries and ice: a positive-negative estuarine couple. In: Lewis, E.L., Jones, E.P., Lemke, P., Prowse, T.D., Wadhams, P. (Eds.), The Freshwater Budget of the Arctic Ocean, NATO Science Partnership Sub-Series: 2, vol. 70. Kluwer Academic, Netherlands, pp. 383–407.
- McIntosh, P.C., 1990. Oceanographic data interpolation: objective analysis and splines. *J. Geophys. Res.* 95 (C8), 13,529.
- Morison, J., Steele, M., Kikuchi, T., Falkner, K., Smethe, W., 2006. Relaxation of central Arctic Ocean hydrography to pre-1990s climatology. *Geophys. Res. Lett.* 33, L17604. doi:10.1029/2006GL026826.
- Morison, J.H., Steele, M., Andersen, R., 1998. Hydrography of the upper Arctic Ocean measured from the nuclear submarine USS Pargo. *Deep-Sea Res. I* 45, 15–38.
- Newton, R., Schlosser, P., Martinson, D.G., Maslowski, W., 2008. Freshwater distribution in the Arctic Ocean: simulation with a high resolution model and model-data comparison. *J. Geophys. Res.* 113, C05024. doi:10.1029/2007JC004111.
- Owens, W.B., Wong, A., 2009. An improved calibration method for the drift of the conductivity sensor on autonomous CTD profiling floats by -S climatology. *Deep-Sea Res. I* 56 (3), 450.
- Pacanowski, R.C., 1995. MOM 2 Documentation, users guide and reference manual, GFDL Ocean Group Technical Report 3, Geophys. Fluid Dyn. Lab., Princeton University, Princeton, NJ.
- Polyakov, I.V., Alexeev, V., Belchansky, F.I., Dmitrenko, I.A., Ivanov, V., Kirillov, S., Koralev, A., Steele, M., Timokhov, L.A., Yashayaev, I., 2008. Arctic Ocean freshwater changes over the past 100 year and their causes. *J. Climate* 21 (2).
- Proshutinsky, A.Y., Johnson, M.A., 1997. Two circulation regimes of the wind-driven Arctic Ocean. *J. Geophys. Res.* 102, 12,493–12,514.
- Proshutinsky, A., Krishfield, R., Timmermans, M.-L., Toole, J., Carmack, E., McLaughlin, F., Williams, W.J., Zimmermann, S., Itoh, M., Shimada, K., 2009. Beaufort Gyre freshwater reservoir: state and variability from observation. *J. Geophys. Res.* 114. doi:10.1029/2008JC005104.
- Rabe, B., Mackensen, A., Schauer, U., Karcher, M., Hansen, E., Beszczynska-Möller, A., 2009. Freshwater components and transports in the FRAM Strait: recent observations and changes since the late 1990s. *Ocean Sci.* 5, 219–233. doi:10.5194/os-5-219-2009.
- Rennermalm, A.K., Wood, E.F., Weaver, A.J., Eby, M., Derý, S.J., 2007. Relative sensitivity of the Atlantic meridional overturning circulation to river discharge into Hudson Bay and the Arctic Ocean. *J. Geophys. Res.* 112, G04S45. doi:10.1029/2006JC000330.
- Rudels, R., Jones, E.P., Schauer, U., Ericksson, P., 2004. Atlantic sources of the Arctic Ocean surface and halocline waters. *Polar Res.* 23 (2), 181–208.
- Schauer, U., Fahrbach, E., Østerhus, S., Rohardt, G., 2004. Arctic warming through the Fram Strait: Oceanic heat transport from 3 years of measurements. *J. Geophys. Res.* 109. doi:10.1029/2003JC001823.
- Serreze, M.C., Barrett, A.P., Slater, A.G., Woodgate, R., Aagaard, K., Lammers, R.B., Steele, M., Moritz, R., Meredith, M., Less, C.M., 2006. The large-scale freshwater cycle of the Arctic. *J. Geophys. Res.* 111 (C11). doi:10.1029/2005JC003424.
- Steele, M., Boyd, T., 1998. Retreat of the cold halocline layer in the Arctic Ocean. *J. Geophys. Res.* 103 (C5), 10,419–10,439.
- Steele, M., Morley, R., Ermold, W., 2001. PHC: a global ocean hydrography with a high quality Arctic Ocean. *J. Climate* 14, 2079–2087.
- Steele, M., Morison, J., Ermold, W., Rigor, I., Ortmeyer, M., Shimada, K., 2004. Circulation of summer Pacific halocline water in the Arctic Ocean. *J. Geophys. Res.* 109. doi:10.1029/2003JC002009.

- Stevens, D.P., 1991. On open boundary condition in the United Kingdom 979 Fine-Resolution Antarctic Model. *J. Phys. Oceanogr.* 21, 1494–1499.
- Woodgate, R.A., Aagaard, K., Weingartner, T.J., 2006. Interannual changes in the Bering Strait fluxes of volume, heat and freshwater between 1991 and 2004. *Geophys. Res. Lett.* 33. doi:10.1029/2006GL026931.
- Yamamoto-Kawai, M., McLaughlin, F.A., Carmack, E.C., Nishino, S., Shimada, K., Kurita, N., 2009. Surface freshening of the Canada Basin, 2003–2007: River runoff versus sea ice meltwater. *J. Geophys. Res.* 114, C00A05. doi:10.1029/2008JC005000.
- Yang, J., 2006. The seasonal variability of the Arctic Ocean Ekman transport and its role in the mixed layer heat and salt fluxes. *J. Climate* 19, 5366–5387.